Satellite-based Estimation of the Impacts of Summertime Wildfires on $PM_{2.5}$ concentration in United States

Zhixin Xue[1], Pawan Gupta[2,3], and Sundar Christopher[1]

[1]Department of Atmospheric and Earth Science, The University of Alabama in Huntsville, Huntsville, 35806 AL, USA
[2]STI, Universities Space Research Association (USRA), Huntsville, 35806 AL, USA
[3]NASA Marshall Space Flight Center, Huntsville, AL, 35806, USA

Abstract

Frequent and widespread wildfires in North Western United States and Canada has become the "*new normal*" during the northern hemisphere summer months, which significantly degrades particulate matter air quality in the United States. Using the mid-visible Multi Angle Implementation of Atmospheric Correction (MAIAC) satellite-derived Aerosol Optical Depth (AOD) with meteorological information from the European Centre for Medium-Range Weather Forecasts (ECMWF) and other ancillary data, we quantify the impact of these fires on fine particulate matter concentration ($PM_{2.5}$) air quality in the United States. We use a Geographically Weighted Regression method to estimate surface $PM_{2.5}$ in the United States between low (2011) and high (2018) fire activity years. Ourresults achieve an overall Leave One Out Cross Validation (LOOCV) R^2 value of 0.797 with RMSE between 3~5 $\mu g\, m^{-3}$. Our results indicate that smoke aerosols caused significant pollution changes over half of the United States. We estimate that nearly 29 states have increased $PM_{2.5}$ during the fire active year and 15 of these states have $PM_{2.5}$ concentrations more than 2 times than that of the inactive year. Furthermore, these fires increased the daily mean surface $PM_{2.5}$ concentrations in Washington and Oregon by 38 to 259μgm^{-3} posing significant health risks especially to vulnerable populations. Our results also show that the GWR

model can be successfully applied to $PM_{2.5}$ estimations from wildfires thereby providing useful information for various applications including public health assessment.

1. Introduction

The United States (US) Clean Air Act (CAA) was passed in 1970 to reduce pollution levels and protect public health that has led to significant improvements in air quality (Hubbell et al., 2010; Samet, 2011). However, the northern part of the US continues to experience an increase in surface $PM_{2.5}$ due to fires in North Western United States and Canada (hereafter NWUSC) especially during the summer months and these aerosols are a new source of 'pollution' (Coogan et al., 2019; Dreessen et al., 2016). The smoke aerosols from these fires increase fine particulate matter ($PM_{2.5}$) concentrations and degrade air quality in the United States (Miller et al., 2011). Moreover several studies have shown that from 2013 to 2016, over 76% of Canadians and 69% of Americans were at least minimally affected by wildfire smoke (Munoz-Alpizar et al., 2017). Although wildfire pre-suppression and suppression costs have increased, the number of large fires and the burnt areas in many parts of western Canada and the United States have also increased. (Hanes et al., 2019; Tymstra et al., 2019). Furthermore, in a changing climate, as surface temperature increases and humidity decreases, the flammability of land cover also increases, and thus accelerate the spread of wildfires (Melillo et al., 2014). The accumulation of flammable materials like leaf litter can potentially trigger severe wildfire events even in those forests that hardly experience wildfires (Calkin et al., 2015; Hessburg et al., 2015; Stephens, 2005).

Wildfire smoke exposure can cause small particles to be lodged in lungs that may lead to exacerbations of asthma chronic obstructive pulmonary disease (COPD), bronchitis, heart disease and pneumonia (Apte et al., 2018; Cascio, 2018). According to a recent study, a 10 $\mu g m^{-3}$ increase in $PM_{2.5}$ is associated with a 12.4% increase in cardiovascular mortality (Kollanus et al.,

2016). In addition, exposure to wildfire smoke is also related to massive economic costs due to premature mortality, loss of workforce productivity, impacts on the quality of life and compromised water quality (Meixner and Wohlgemuth, 2004).

Surface $PM_{2.5}$ is one of the most commonly used parameters to assess the health effects of ambient air pollution. Given the sparsity of measurements in many parts of the world, it is not possible to use interpolation techniques between monitors to provide $PM_{2.5}$ estimates on a square kilometer basis. Since surface monitors are limited, satellite data has been used with numerous ancillary data sets to estimate surface $PM_{2.5}$ at various spatial scales. Several techniques have been developed to estimate surface $PM_{2.5}$ using satellite observations from regional to global scales including simple linear regression, multiple linear regression, mixed-effect model, chemical transport model (scaling methods), geographically weighted regression (GWR), and machine learning methods (see Hoff and Christopher, 2009 for a review). The commonly used global satellite data product is the 550nm (mid-visible) aerosol optical depth (AOD) which is a unitless columnar measure of aerosol extinction. Simple linear regression method uses satellite AOD as the only independent variable, which shows limited predictability compared to other methods and correlation coefficients vary from 0.2 to 0.6 from the Western to Eastern United States (Zhang et al., 2009). Multiple linear regression method uses meteorological variables along with AOD data, and the prediction accuracy varies with different conditions including the height of boundary layer and other meteorological conditions (Goldberg et al., 2019; Gupta and Christopher, 2009b; Liu et al., 2005). For both univariate model and multi-variate models, AOD shows stronger correlation with $PM_{2.5}$ during-fire episodes compared to pre-fire and post-fire periods (Mirzaei et al., 2018). Chemistry transport models (CTM) that scale the satellite AOD by the ratio of $PM_{2.5}$ to AOD simulated by models can provide $PM_{2.5}$ estimations without ground measurements, which are

different than other statistical methods (Donkelaar et al., 2019, 2006). However, the CTM models that depend on reliable emission data usually show limited predictability at shorter time scales, and is largely useful for studies that require annual averages (Hystad et al., 2012). Different machine learning methods including neuron network, random forest, and deep belief networks show improvements on prediction accuracy (with CV R^2 values larger than 0.8) which is hard to accomplish for other parametric regression models (Hu et al., 2017; Li et al., 2017; Wei et al., 2021, 2020, 2019). However, these methods also require large amount of samples to train the model which means it is more suitable for daily PM2.5 estimation rather than short-term wildfire events with relative low occurrence frequency.

The relationship among $PM_{2.5}$, AOD and other meteorological variables is not spatially consistent (Hoff and Christopher, 2009; Hu, 2009). Therefore, methods that consider spatial variability can replicate surface $PM_{2.5}$ with higher accuracy. One such method is the GWR, which is a non-stationary technique that models spatially varying relationships by assuming that the coefficients in the model are functions of locations (Brunsdon et al., 1996; Fotheringham et al., 1998, 2003). In 2009, satellite-retrieved AOD was introduced in the GWR method to predict surface $PM_{2.5}$ (Hu, 2009) followed by the use of meteorological parameters and land use information (Hu et al., 2013). Meteorological variables are crucial for simulating surface $PM_{2.5}$ since they interact with $PM_{2.5}$ through different processes which will be discussed in detail in the data section (Chen et al., 2020). Several studies (Guo et al., 2021; Ma et al., 2014; You et al., 2016a) successfully applied the GWR model in estimating $PM_{2.5}$ in China by using AOD and meteorological features as predictors. Similar to all the statistical methods, however, the GWR relies on adequate number and density of surface measurements (Chu et al., 2016; Gu, 2019; Guo et al., 2021), underscoring the importance of adequate ground monitoring of surface $PM_{2.5}$.

In this paper, we use satellite data from the Moderate Resolution Imaging Spectroradiometer (MODIS) and surface $PM_{2.5}$ data combined with meteorological and other ancillary information to develop and use the GWR method to estimate $PM_{2.5}$. The use of the GWR method is not novel and we merely use a proven method to estimate surface $PM_{2.5}$ from forest fires. We calculate the change in $PM_{2.5}$ between a high fire activity (2018) with low fire activity (2011) periods during summer to assess the role of NWUSC wildfires on surface $PM_{2.5}$ in the United States. The paper is organized as follows: We describe the data sets used in this study followed by the GWR method. We then describe the results and discussion followed by a summary with conclusions.

2. Data

A 17-day period (August 9th to August 25th) in 2018 (high fire activity) and 2011 (low fire activity) was selected based on analysis of total fires (details in methodology section) to assess surface $PM_{2.5}$ (Table 1).

2.1 Ground level $PM_{2.5}$ observations: Daily surface $PM_{2.5}$ from the Environment Protection Agency (EPA) are used in this study. These data are from Federal Reference Methods (FRM), Federal Equivalent Methods (FEM), or other methods that are to be used in the National Ambient Air Quality Standards (NAAQS) decisions. A total of 1003 monitoring sites in the US are included in our study with 949 having valid observations in the study period in 2018, and a total of 873 sites with 820 having valid observations in the study period in 2011. $PM_{2.5}$ values less than 2 μgm^{-3} are discarded since they are lower than the established LDL-Lower Detection Limit (EPA, 2018, 2011).

2.2 Satellite Data: AOD which represents the total column aerosol mass loading is related to surface $PM_{2.5}$ as a function of aerosol vertical properties and physical properties (Koelemeijer et al., 2006):

$$AOD = PM_{2.5}\ H\ f(RH)\frac{3Q_{ext,dry}}{4\rho\ r_{eff}} = PM_{2.5}\ H\ S \quad (1)$$

Where H is the aerosol layer height, f(RH) is the ratio of ambient and dry extinction coefficients, $Q_{ext,dry}$ is the extinction efficiency under dry conditions, r_{eff} is the particle effective radius, ρ is the aerosol mass density and S is the specific extinction efficiency ($m^2\ g^{-1}$) of the aerosol at ambient conditions. Therefore AOD usually has a strong positive correlation with $PM_{2.5}$, and the relationship varies depending on other meteorological parameters which will be discussed in detail in the following section.

The MODIS mid visible AOD from the Multi-Angle Implementation of Atmospheric Correction (MAIAC) product (MCD19A2 Version 6 data product) is used in this study. We used the MAIAC- retrieved Terra and Aqua MODIS AOD product at 1 km pixel resolution (Lyapustin et al., 2018). Different orbits are averaged to obtain mean daily values. Since thick smoke plumes generated by wildfires can be misclassified as cloud, we preserve possible cloud contaminated pixels to preserve the thick smoke pixels, and only AOD less than 0 will be discarded. Validation with AERONET studies show that 66% of the MAIAC AOD data agree within ±0.5~±0.1 AOD (Lyapustin et al., 2018). Largely due to cloud cover, grid cells may have limited number of AOD observations within a certain period. On average, cloud free AOD data are available about 40% of the time during August 9th to August 25th in 2018 when fires were active in the region bounded by 25~50°N, 65~125°W. Smoke flag from the same product is used as a predictor in estimating surface $PM_{2.5}$. The smoke detection is performed using MODIS red, blue and deep blue bands, and

137 smoke pixels are separated from dust and clouds based on absorption parameter, size parameter
138 and thermal thresholds (see Lyapustin et al., 2012; 2018 for further discussion). Smoke flag data
139 can provide the percentage of smoke pixel in each grid, which is related to smoke coverage.

140 We also use the MODIS level-3 daily FRP (MCD14ML, fire radiative power) product
141 which combines Terra and Aqua fire products to assess wildfire activity. The fire radiative energy
142 indicates the rate of combustion and thus FRP can be used for characterizing active fires (Freeborn
143 et al, 2014). For purposes of the study we sum the FRP within every 2.3°×3.5° box to represent
144 the total fire activity in different locations.

145 **2.3 Meteorological data:** Meteorological information including boundary layer height (BLH), 2m
146 temperature (T2M), 10m wind speed (WS), surface relative humidity (RH) and surface pressure
147 (SP) are obtained from the European Centre for Medium-Range Weather Forecasts (ECMWF)
148 reanalysis (ERA5) product, with a spatial resolution of 0.25 degrees and temporal resolution of 1
149 hour and is matched temporally with the satellite overpass time. The meteorological parameters
150 provide important information of different processes affecting surface $PM_{2.5}$ concentration, which
151 can also be seen as supplements of the AOD-$PM_{2.5}$ relationship as previously discussed.

152 The BLH can provide information of aerosol layer height (H in equation 1) as aerosols are often
153 found to be well-mixed within the boundary layer (Gupta and Christopher, 2009b). With same
154 amount of pollution within the boundary layer, the higher the BLH is, the more $PM_{2.5}$ is distributed
155 within that layer and vice-versa (Miao et al., 2018; Zheng et al., 2017). Therefore, $PM_{2.5}$ usually
156 has an anticorrelation with BLH. However, for wildfire events, the aerosol layer height is
157 sometimes higher than the BLH (Haarig et al., 2018), which leads to lower correlation between
158 AOD and $PM_{2.5}$ since we use only BLH to present the aerosol layer height. Thus BLH can provide
159 aerosol vertical information in most cases except for suspended high-layer aerosol caused by fires,

which leads to higher bias of the model for high-layer aerosols near the fire sources. Surface temperature (T2M) can affect $PM_{2.5}$ through convection, evaporation, temperature inversion and secondary pollutants generation processes (Chen et al., 2020). The first two processes are negatively related to $PM_{2.5}$ concentration: 1) higher temperature increases turbulence and atmospheric convections which accelerate the pollution dispersion ($PM_{2.5}$ decreases); 2) higher temperature increases evaporation loss of $PM_{2.5}$ including ammonium nitrate and other volatile or semi-volile components (Wang et al., 2017). The later two processes are positively related to $PM_{2.5}$ by limiting vertical motion and promoting photochemical reactions under high temperature (Xu et al., 2019; Zhang et al., 2015). Wind speed (WS) are often negatively related to $PM_{2.5}$ since it increases the dispersion of pollutants. However, unique geographical conditions (such like mountains) with certain wind directions can cause accumulations of pollutants (Chen et al., 2017). RH may promote hygroscopic growth of particles to increase $PM_{2.5}$ (Trueblood et al., 2018; Zheng et al., 2017), but it can also reduce $PM_{2.5}$ through the deposition process. SP may influence the diffusion or accumulation of pollutants through formation of low-level wind convergence (You et al., 2017). Precipitation is another factor that largely influences surface $PM_{2.5}$ since it can accelerate the wash-out of suspended particles, but AOD values are not available when clouds are present.

3. Methodology

To assess the impact of NWUSC fires on $PM_{2.5}$ in the United States, we first estimate the $PM_{2.5}$ over the study region during a time period with high fire activity (2018). We then use the same method during a year with low fire activity (2011) to compare the differences between the two years. The two years are selected based on the total FRP in August calculated within Canada (49~60°N, 55~135°W) and Northwestern (NW) US (35~49°N, 105~125°W). Table 2 shows the

total FRP in Canada and Northwestern US in August from 2010 to 2018. The total FRP in the two regions is lowest in 2011 and highest in 2018 during the 9 years, which provides the basis for the study. In order to create a 0.1° surface $PM_{2.5}$, the GWR model is used to estimate the relationships of $PM_{2.5}$ and AOD. Detailed processing steps for GWR model are shown in Figure 1.

3.1 Data preprocessing: The first step is to resample all datasets to a uniform spatial resolution by creating a 0.1° resolution grid covering the Continental United States. During this process, we collocate the $PM_{2.5}$ data and average the values if there is more than one value in one grid. Then the MAIAC AOD and smoke flagare averaged into 0.1° grid cells. Meteorological datasets are also resampled to the 0.1° grid cells by applying the inverse distance method.

3.2 Time selecting & averaging: Next we select data where AOD and ground $PM_{2.5}$ are both available (AOD > 0 and $PM_{2.5} > 2.0\ \mu g\ m^{-3}$) and average them for the study period (since LDL of for the FRM method is $2\ \mu g\ m^{-3}$ in 2011 and $3\ \mu g\ m^{-3}$ in 2018, we decides to use the LDL for 2011) (EPA, 2018, 2011). This is to ensure that the AOD, $PM_{2.5}$ and other variables match with each other, because $PM_{2.5}$ is not a continuous measurement for some sites and AOD have missing values due to cloud cover and other reasons. Therefore, it is important to use data from days where both measurements are available to avoid sampling biases.

3.3 GWR model development and validation: The Adaptive bandwidth selected by the Akaike's Information Criterion (AIC) is used for the GWR model (Loader, 1999). For locations that already have $PM_{2.5}$ monitors, we calculate the mean AOD of a 0.5×0.5° box centered at the ground location and estimate the GWR coefficients (β) for AOD and meteorological variables to estimate $PM_{2.5}$. The model structure can be expressed as:

$$PM_{2.5i} = \beta_{0,i} + \beta_{1,i}AOD_i + \beta_{2,i}BLH_i + \beta_{3,i}T2M_i + \beta_{4,i}U10M_i + \beta_{5,i}RH_{sfci} + \beta_{6,i}SP_i + \beta_{7,i}SF_i + \varepsilon_i$$

where $PM_{2.5i}$ ($\mu g\ m^{-3}$) is the selected ground-level $PM_{2.5}$ concentration at location i; $\beta_{0,i}$ is the intercept at location i; $\beta_{1,i}$~$\beta_{8,i}$ are the location-specific coefficients; AOD_i is the resampled AOD selected from MAIAC daily AOD data at location i; $BLH_i, T2M_i, U10M_i, RH_{sfci}, SP_i$ are selected meteorological parameters (BLH, T2M, WS, RH and PS) at location i; SF_i (%) is the resampled smoke flag data at location i and ε_i is the error term at location i.

We perform the Leave One Out Cross Validation (LOOCV) to test the model predictive performance (Kearns and Ron, 1999). Since the GWR model relies on adequate number of observations, the prediction accuracy will be lower if we preserve too much data for validation. Therefore, we choose the LOOCV method, which preserve only one data for validation at a time and repeat the process until all the data are used. In addition, R^2 and RMSE are calculated for both model fitting and model validation process to detect overfitting. Model overfitting will lead to low predictability, which means it fits too close to the limited number of data to predict for other places and will cause large bias.

3.4 Model prediction: While predicting the ground-level $PM_{2.5}$ for unsampled locations, we make use of the estimated parameters for sites within a 5° radius to generate new slopes for independent variables based on the spatial weighting matrix (Brunsdon et al., 1996). The closer to the predicted location, the closer to 1 the weighting factor will be, while the weighting factor for sites further than the 5° in distance is zero. It is important to note that AOD and other independent variables used for prediction in this step are averaged values for days that have valid AOD, which is different from the data used in the fitting process since $PM_{2.5}$ is not measured every day in all locations.

4. Results and Discussion

We first discuss the surface $PM_{2.5}$ for a few select locations that are impacted by fires followed by the spatial distribution of MODIS AOD and the FRP for August 2018. We then assess the spatial distribution of surface $PM_{2.5}$ from the GWR method. The validation of the GWR method is then discussed. To further demonstrate the impact of the NWUSC fires on $PM_{2.5}$ air quality in the United States, we show the spatial distribution of the difference between August 2018 and August 2011. We further quantify these results for ten US EPA regions.

4.1 Descriptive statistics of satellite data and ground measurements

The 2018 summertime Canadian wildfires started around the end of July in British Columbia and continued until mid-September. The fires spread rapidly to the south of Canada during August, causing high concentrations of smoke aerosols to drift down to the US and affecting particulate matter air quality significantly. From late July to mid-September, wildfires in the northwest US that burnt forest and grassland also affected air quality. Starting with the Cougar Creek Fire, then Crescent Mountain and Gilbert Fires, different wildfires in in NWUSC caused severe air pollution in various US cities. Figure 2a shows the rapid increase in $PM_{2.5}$ of selected US cities from July 1st to August 31st, due to the transport of smoke from these wildfires. For all sites, July had low $PM_{2.5}$ concentrations (<10 $\mu g\, m^{-3}$) and rapidly increases as fire activity increases. Calculating only from the EPA ground observations, the mean $PM_{2.5}$ of the 17 days for the whole US is 13.7 $\mu g\, m^{-3}$ and the mean $PM_{2.5}$ for Washington (WA) is 40.6$\mu g m^{-3}$, which indicates that the PM pollution is concentrated in the northwestern US for these days. This trend is obvious when comparing the mean $PM_{2.5}$ of all US stations (black line with no markers) and the mean $PM_{2.5}$ of all WA stations (grey line with no markers). Ground-level $PM_{2.5}$ reaches its peak between August 17th-21st and daily $PM_{2.5}$ values during this time period far exceeds the 17-day

mean $PM_{2.5}$. For example, mean $PM_{2.5}$ in WA on August 20th is 86.75 $\mu g\ m^{-3}$, which is more than two times the 17-day average of this region. On August 19th, Omak which is located in the foothills of the Okanogan Highlands in WA had $PM_{2.5}$ values exceed 250 $\mu g\ m^{-3}$. According to a review of US wildfire caused $PM_{2.5}$ exposures, 24-h mean $PM_{2.5}$ concentrations from wildfires ranged from 8.7 to 121 $\mu g\ m^{-3}$, with a 24 h maximum concentration of 1659 $\mu g\ m^{-3}$ (Navarro et al., 2018).

Table 3 shows relevant statistics of 15 states that have at least one daily record of non-attainment of EPA standard (>35 μg m^{-3} . From the frequency records of non attainment in the 17-day period (last column), four states (Montana, Washington, California and Idaho) were consistently affected by the wildfires, and large portion of ground stations in these states were influenced by smoke aerosols. Most of the neighboring states also suffered from short-term but broad air pollution (third column). Noticeable from these records is that the total number of ground stations in some of the highly affected states (such as Idaho) is not sufficient for capturing the smoke. Although there are total 8 EPA stations in Idaho, only two of them have consistent observations during the fire event; the other two stations have no valid observations, and the remaining four stations have only 2~6 observations during the 17-day period. Limited valid data along with unevenly distributed stations makes it hard to quantify smoke pollution in Northwestern US during the fire event period. Therefore, we utilize satellite data to enlarge the spatial coverage and estimate pollution at a finer spatial resolution.

The spatial distribution of AOD shown in Figure 2b indicates that the smoke from Canada is concentrated mostly in Northern US states such as WA, Oregon, Idaho, Montana, North Dakota and Minnesota. The black arrow shows the mean 800hPa-level mean wind for 17 days, and the length of the arrow represents the wind speed in ms^{-1}. Also shown in Figure 2b are wind speeds

close to the fire sources which are about 4~5 ms^{-1}, and according to the distances and wind directions, it can take approximately 28~36 hours for the smoke to transport southeastward to Washington state. Then the smoke continues to move east to other northern states such as Montana and North Dakota. In addition, the grey circle represents the total fire radiative power (FRP) of every 2.3×3.5-degree box. The reason for not choosing a smaller grid for the FRP is to not clutter Figure 2b with information from small fires. The bigger the circle is, the stronger the fire is in that grid and different sizes and its corresponding FRP values are shown in the lower right corner. It is clear that the strongest fires in 2018 are located in the Tweedsmuir Provincial Park of British Columbia in Canada (53.333N, 126.417W). The four separate lightning-caused wildfires burnt nearly 301,549 hectares of the boreal forest. The total FRP of August 2018 in Canada is about 5362 (*1000 MW), while the total FRP of August 2011 in Canada is 48 (* 1000 MW). The 2011 fire was relatively weak compared to the 2018 Tweedsmuir Complex fire and we therefore use the 2011 air quality data as a baseline to quantify the 2018 fire influence on $PM_{2.5}$ in the United States.

4.2 Model Fitting and validation

The main goal for using GWR model is to help predict the spatial distribution of $PM_{2.5}$ for places with no ground monitors while leveraging the satellite AOD and therefore it is important to ensure that the model is robust. Figure 3a and 3b show the results for 2018 for GWR model fitting for the entire US and the LOOCV models respectively. The color of the scatter plots represents the probability density function (PDF) which calculates the relative likelihood that the observed ground-level $PM_{2.5}$ would equal the predicted value. The lighter the color is, the more points are present, with a higher correlation. The model fitting process estimates the slope for each variable and therefore the model can be fitted close to the observed $PM_{2.5}$ and using this estimated relationship we are able to assess surface $PM_{2.5}$ using other parameters at locations where $PM_{2.5}$

monitors are not available. The LOOCV process tests the model performance in predicting $PM_{2.5}$. If the results of LOOCV has a large bias from the model fitting, then the predictability of the model is low. Higher R^2 difference and RMSE difference value indicate that the model is overfitting and not suitable. The R^2 for the model fitting is 0.834, and the R^2 for the LOOCV is 0. 797; the RMSE for the GWR model fitting is 3.46 $\mu g\ m^{-3}$, and for LOOCV the RMSE is 3.84 $\mu g\ m^{-3}$. There are minor differences between fitting R^2 and validation R^2 (0.037) and between fitting RMSE and validation RMSE (0.376 $\mu g\ m^{-3}$) suggesting that the model is not over-fitting and has stable predictability further indicating that the model can predict surface $PM_{2.5}$ reliably. In addition, we also performed a 20-fold cross validation by splitting the dataset into 20 consecutive folds, and each fold is used for validation while the 19 remaining folds form the training set. The 20-fold cross validation has R^2 of 0.745 and RMSE of 4.3 $\mu g\ m^{-3}$. The increase/decrease in the cross validated R^2 and RMSE indicates the importance of sufficient data used for fitting since a small decrease in the number of fitting data can reduce the model prediction accuracy. Overall, the prediction error of the model is between 3~5 $\mu g\ m^{-3}$, which is a reasonable error range for 17-day average prediction of $PM_{2.5}$. For data greater than the EPA standard (35 $\mu g\ m^{-3}$), the model has a RMSE of 12.07 $\mu g\ m^{-3}$, which is a lot larger than the RMSE when using the entire model. Therefore, the model has a tendency for underestimating $PM_{2.5}$ exceedances by around 12.07 $\mu g\ m^{-3}$. The larger the $PM_{2.5}$ is, the greater the model underestimates. To examine the model performance for high and low polluted areas, the results are divided into two parts (larger than 35 $\mu g\ m^{-3}$ and less than 35 $\mu g\ m^{-3}$). Aeras with high pollution have R^2 of 0.64 and areas with low pollution have R^2 of 0.67, therefore, the model performance is relative stable for both large and small $PM_{2.5}$ values. Also, the inclusion of low aerosol concentration areas does not influence the model performance for high values (seen in supplemental material in igures S1 and S2), which

means that the high R^2 is not a reason of large number of low values. The GWR model fitting and validation results for the 17 days in 2011 are shown in figure S3.

4.3 Predictors' influence during wildfires

Table 4 shows the GWR model mean coefficients for the whole US region and for different selected regions. The selected boxes are shown in figure 4c in different colors: box1 (red) located in NW US include major fire sources in US; box2 (gold) located in Montana state is influenced from both neighboring states and smoke from Canada; box3 (green) in Minnesota which is located further from the fires and has minor increase in $PM_{2.5}$ due to remote smoke; box4 (black) in NE (Northeast) US is the furthest from fires and has no obvious pollution increase. The second column of the tables shows the conditions for sample selection and the third column shows the number of pixels selected for each box. By comparing the coefficients of samples selected in these boxes, predictors have different influence in different locations. AOD has stronger influence on predicting $PM_{2.5}$ closer to fire sources, but local emissions become more dominant if the distances is large enough. The smoke flag is overall positive related to surface $PM_{2.5}$, while it could slightly negatively relate to $PM_{2.5}$ around fire sources and northeastern coasts. PBL is negatively related to $PM_{2.5}$ when the pollution is concentrated near the surface (fires or human-made emissions), while it appears to be positively related to $PM_{2.5}$ at locations where the main pollution source comes from remote wildfire smoke. Surface temperature have a relative stable positive correlation with surface $PM_{2.5}$, however, surface pressure and wind speeds are negatively correlated with $PM_{2.5}$. Relative humidity, on the other hand, shows large variations on $PM_{2.5}$ influence across the nation. Around the wildfires where the RH is relative low, RH has a positive correlation with $PM_{2.5}$ since hygroscopicity would increase and leads to accumulation of $PM_{2.5}$, but increasing RH can also

decrease $PM_{2.5}$ concentration by overgrowing the $PM_{2.5}$ particles to deposition at high RH environment (Chen et al., 2018).

From table 4, we know that the weighting for AOD is much larger than other predictors, but predictors other than AOD are important for the prediction. We tested our model with AOD as the only predictor to conduct a comparison with the original model, and the R^2 decreases from 0.83 to 0.79 and RMSE increases from 3.46 to 3.8. This is consistent with previous study (Jiang et al., 2017) which shows improvements of R^2 from 0.69 to 0.78 and RMSE from 7.25 to 6.18 by adding 4 meteorological parameters in summer in easter China. Other predictors have higher weighting at the fire source region (box1) where BLH cannot provide the aerosol vertical distribution information since smoke tends to be injected to higher levels. For high AOD regions where aerosol tends to be suspended at high levels, adding other predictors other than AOD tends to have lower improvement of the model compared with low AOD values, because adding BLH can significantly improve the prediction for low level aerosols. For regions with AOD less than 35, R^2 increases 0.09 from AOD only model (0.6 to 0.69), while R^2 increases 0.05 for areas with AOD larger than 35. RMSE decreases 12% and 7% for AOD less and larger than 35 conditions, respectively. Overall, the meteorological factors have larger improvements for low polluted areas (low level aerosol in this case).

4.4 Predicted $PM_{2.5}$ Distribution

The mean $PM_{2.5}$ distributions over the United States shown in Figure 4a is calculated by averaging the surface $PM_{2.5}$ data from ground monitors for the 17 days, which matches well with the GWR model-predicted $PM_{2.5}$ distributions shown in Figure 4b. The model estimation extends the ground measurements and provide pollution assessments across the entire nation. Comparing the AOD map (Figure 2b) with the $PM_{2.5}$ estimations (Figure 4b), demonstrates the differences between columnar and surface-level pollution. Differences between the AOD and $PM_{2.5}$

363 distributions are due to various reasons including 1) Areas with high $PM_{2.5}$ concentrations in figure
364 4b correspond to low AOD values in figure 2b (Southern California, Utah, and southern US); 2)
365 and high AOD regions in figure 2b correspond to low $PM_{2.5}$ concentrations in figure 4b
366 (Minnesota). The first situation usually occurs at the edge of polluted areas that are relative far
367 from the fire source, which is consistent with previous studies that reported smaller particles (<10
368 μg) are able to travel longer distances compared to large particles (>10 μg) (Gillies et al., 1996),
369 and that lager particles tend to settle closer to their source (Sapkota et al., 2005; Zhu et al., 2002).

370 We use the same method for August 9th to August 25th in 2011 that had low fire activity,
371 ensuring consistency for estimating coefficients for different variables for 2011. Figure 4c shows
372 the difference in spatial distribution of mean ground $PM_{2.5}$ of the 17 days between 2018 and 2011.
373 High values of $PM_{2.5}$ differences are in the Northwestern and central parts of the United States
374 with the Southern states having very little impact due to the fires. Of all the 48 states within the
375 study region, there are 29 states that have a higher $PM_{2.5}$ value in 2018 than 2011, and 15 states
376 have 2018 $PM_{2.5}$ value more than two times their 2011 value (shown in figure 5). The mean $PM_{2.5}$
377 for WA increases from 5.87 in 2011 to 46.47 $\mu g\ m^{-3}$ in 2018, which is about 8 times more than
378 2011 values. The $PM_{2.5}$ values in Oregon increases from 4.97 (in 2011) to 33.3 $\mu g\ m^{-3}$ in 2018,
379 which is nearly seven times more than in 2011. For states from Montana to Minnesota, the mean
380 $PM_{2.5}$ decreases from east to west, which reveals the path of smoke transport. As shown in Figure
381 4c, there is a clear transport path of smoke from North Dakota all the way to Texas. Along the
382 path, smoke increases $PM_{2.5}$ concentrations by 168% in North Dakota and 27% in Texas. Smoke
383 aerosols transported over long distances contains fine fraction PM which significantly affect the
384 health of children, adults, and vulnerable groups.

Figure 5 shows the mean $PM_{2.5}$ predicted from the GWR model of different EPA regions for the 17 days in 2011 and 2018 (Hawaii and Alaska are not included). The most influenced region is region 10, which has a 2018 mean $PM_{2.5}$ value of 34.2 $\mu g\ m^{-3}$ that is 6 times larger than the values in 2011 (5.8 $\mu g\ m^{-3}$) values. The $PM_{2.5}$ of region 8 and 9 have 2.4 and 2.6 times increase in 2018 compared to 2011. Region 1~4 have lower $PM_{2.5}$ in 2018 than 2011 possibly due to Clean Air Act initiatives, absence of any major fire activites and further away for transported aerosols. The emission reduction improves the US air quality and lower the $PM_{2.5}$ every year, but 6 out of 10 EPA regions show significant increases in $PM_{2.5}$ during the study period, which indicates that the long-range transported wildfire smoke has become the new major pollutant in the US.

4.5 Estimation of Canadian fire pollution

To evaluate the pollution caused only from Canadian fires, we did a rough assessment according to the total FRP and $PM_{2.5}$ values. There are three states in the US have wildfires during the study period: California, Washington and Oregon, and they have total FRP of 1186, 518 and 439 (*1000 MW) respectively. Assuming that California was only influenced by the local fires, then fires of 1186 (*1000 MW) cause 13 $\mu g\ m^{-3}$ increase in $PM_{2.5}$. Accordingly, wildfires in Washington and Oregon State will cause 6 and 5 $\mu g\ m^{-3}$ increase in state mean $PM_{2.5}$. Therefore, Canadian fires caused $PM_{2.5}$ increase in Washington and Oregon is about 35 and 23 $\mu g\ m^{-3}$. Since the FRP of Canadian wildfires are approximately 5 times larger than that of the California fires, which is the strongest fire in US, we assume the pollution affecting the states located in the downwind directions other than the three states are mainly coming from Canadian wildfires. States with no local fires such as Montana, North Dakota, South Dakota and Minnesota have $PM_{2.5}$ increase of 18.31, 12.8, 10.4 and 10.13 $\mu g\ m^{-3}$. The decrease of these numbers reveal that the smoke is transport in a SE direction. This influence of Canadian wildfires on US air quality is only

a rough quantity estimation, thus additional work is needed for understand long-range transport smoke pollution and its impact on public health. One way to do this would be assessing the difference of pollution by turning on and off US fires in chemistry models.

4.6 Comparison with previous studies

Comparing with the Bayesian ensemble model developed by Geng et al. (Geng et al., 2018) using MAIAC AOD and CMAQ (Community Multiscale Air Quality) model and ground $PM_{2.5}$ measurements, our GWR model has larger R^2, but with the chemistry transport model (CTM), their method can provide more vertical distribution information which is important for wildfire smoke. GWR usually have better accuracy than CTM since there are large uncertainties related to different CTM inputs such as emission, meteorological and land cover data, but for regions with less or no ground measurements, CTM provide a great approach for estimating surface $PM_{2.5}$. Other studies which used machine learning method to predict surface $PM_{2.5}$ have better performance for long-term prediction rather than monthly estimation (Liang et al., 2020; Xiao et al., 2018), but can better resolve complex relationship between different predictors than statistical models (Geng et al., 2020). For wildfire events, the available data is much less than the long-term aerosol analysis, so the performance of machine learning method could be less accurate compared to long-term prediction. Our study also shows slightly larger R^2 compared to other GWR studies (Hu et al., 2013; Ma et al., 2014; You et al., 2016b) due to the inclusion of more meteorological and other related predictors.

4.7 Model uncertainties and limitations

There are various sources of uncertainties and limitations for studies that use satellite data to estimate surface $PM_{2.5}$ concentrations. Since wildfires develop quickly it is important to have

continuous observations to capture the rapid changes. This study uses polar orbiting high-quality satellite aerosol products, but the temporal evolution can only be estimated by geostationary data sets. Although satellite observations have excellent spatial coverage, missing data due to cloud cover is a limitation. As discussed in the paper, the prediction error (RMSE) of the model is between 3~5 $\mu g\ m^{-3}$, while the RMSE increased for locations with high aerosol concentration. This is partly due to lack of accurate vertical distribution information which is very important for wildfire smoke. The GWR model is largely influenced by the distribution of ground stations, and the prediction error will be different in different places due to unevenly distributed $PM_{2.5}$ stations. For locations that have a dense ground-monitoring distribution, the prediction error will be low, while the prediction error will be relative larger at other places with sparse surface stations. Although there are obvious limitations, complementing surface data with satellite products and meteorological and other ancillary information in a statistical model like the GWR has provided robust results for estimating surface $PM_{2.5}$ from wildfires. We also note that we did not consider some variables used in other studies such as NDVI, forest cover, vegetation type, industrial density, visibility and chemical constituents of smoke particles (Donkelaar et al., 2015; Hu et al., 2013; You et al., 2015; Zou et al., 2016). Visibility mentioned in some studies may improve the model performance, but unlike AOD, it has limited measurement across the nation, which will restrict the applicability of training data. Another uncertainty comes from the 2011 wildfires which we assumed to be zero fire events but there are actually few fire events in EPA region 6, 8, 9 and 10, and this will lead to underestimation of $PM_{2.5}$ increase due to 2018 fires in these regions.

One limitation of this study is that analysis based on 17-day mean values cannot capture daily pollution variations, which is also very important for pollution estimation during rapid-changing wildfire events. To extend this analysis to daily estimation, the cloud contaminations of

satellite observations become a major problem. Therefore, future work is needed using chemistry transport models and other data to fill in the gaps on missing AOD data due to cloud coverage.

5. Summary and Conclusions

We estimate the surface mean $PM_{2.5}$ for 17 days in August for a high fire active year (2018) and compare that with a low fire activity year using the Geographically Weighted Regression (GWR) method to assess the increase in $PM_{2.5}$ in the United States due to smoke transported from fires. The difference in $PM_{2.5}$ between the two years indicates that more than half of the US states (29 states) are influenced by the NWUSC wildfires, and half of the affected states have 17-day mean $PM_{2.5}$ increases larger than 100% of the baseline value. The peak $PM_{2.5}$ during the wildfires can be much larger than the 17-day average and can affect vulnerable populations susceptible to air pollution. Some of the most affected states are in Washington, California, Wisconsin, Colorado and Oregon, all of which have populations greater than 4 million. According to CDC (Centers for Disease Control and Prevention), 8% of the population have asthma (CDC, 2011). Therefore, for asthma alone, there are about 3 million people facing significant health issue due to the long-range transport smoke in these states.

For states that show decrease in $PM_{2.5}$ due to the Clean Air Act, the mean decrease is about 16% of the baseline after 7 years. This is consistent with EPA's report that there is a 23% decrease of $PM_{2.5}$ in national average from 2010 to 2019(U.S. Environmental Protection Agency, 2019). Comparing with the dramatic increase (132%) caused by wildfires, pollution from the fires is counteracting our effort on emission controls. Although wildfires are often episodic and short-term, high frequency of fire occurrence and increasing longer durations of summertime wildfires in recent years has made them now a long-term influence on public lives. Our results show a significant increase of pollution in a short time period in most of the US states due to the NWUSC

476 wildfires, which affects millions of people. With wildfires becoming more frequent during recent
477 years, more effort is needed to predict and warn the public about the long-range transported smoke
478 from wildfires.

479 **Acknowledgements.**

480 Pawan Gupta was supported by a NASA Grant. MODIS data were acquired from the Goddard
481 DAAC. Sincerest thanks to the MAIAC, MODIS, EPA and ECMWF teams for their datasets that
482 makes this research possible.

483 **References**

484 Apte, J.S., Brauer, M., Cohen, A.J., Ezzati, M., Pope, C.A., 2018. Ambient PM2.5 Reduces
485 Global and Regional Life Expectancy. Environ. Sci. Technol. Lett. 5, 546–551.
486 https://doi.org/10.1021/acs.estlett.8b00360

487 Brunsdon, C., Fotheringham, A.S., Charlton, M.E., 1996. Geographically Weighted Regression:
488 A Method for Exploring Spatial Nonstationarity. Geogr. Anal. 28, 281–298.
489 https://doi.org/https://doi.org/10.1111/j.1538-4632.1996.tb00936.x

490 Calkin, D.E., Thompson, M.P., Finney, M.A., 2015. Negative consequences of positive
491 feedbacks in us wildfire management. For. Ecosyst. 2, 1–10.
492 https://doi.org/10.1186/s40663-015-0033-8

493 Cascio, W.E., 2018. Wildland Fire Smoke and Human Health. Sci. Total Environ. 624, 586–595.
494 https://doi.org/10.1016/j.scitotenv.2017.12.086.

495 CDC, 2011. Asthma in the US. CDC Vital Signs 1–4.

496 Chen, D., Xie, X., Zhou, Y., Lang, J., Xu, T., Yang, N., Zhao, Y., Liu, X., 2017. Performance

497 evaluation of the WRF-chem model with different physical parameterization schemes
498 during an extremely high PM2.5 pollution episode in Beijing. Aerosol Air Qual. Res. 17,
499 262–277. https://doi.org/10.4209/aaqr.2015.10.0610

500 Chen, Z., Chen, D., Zhao, C., Kwan, M. po, Cai, J., Zhuang, Y., Zhao, B., Wang, X., Chen, B.,
501 Yang, J., Li, R., He, B., Gao, B., Wang, K., Xu, B., 2020. Influence of meteorological
502 conditions on PM2.5 concentrations across China: A review of methodology and
503 mechanism. Environ. Int. 139, 105558. https://doi.org/10.1016/j.envint.2020.105558

504 Chen, Z., Xie, X., Cai, J., Chen, D., Gao, B., He, B., Cheng, N., Xu, B., 2018. Understanding
505 meteorological influences on PM2.5 concentrations across China: A temporal and spatial
506 perspective. Atmos. Chem. Phys. 18, 5343–5358. https://doi.org/10.5194/acp-18-5343-2018

507 Chu, Y., Liu, Y., Li, X., Liu, Z., Lu, H., Lu, Y., Mao, Z., Chen, X., Li, N., Ren, M., Liu, F., Tian,
508 L., Zhu, Z., Xiang, H., 2016. A review on predicting ground PM2.5 concentration using
509 satellite aerosol optical depth. Atmosphere (Basel). 7, 129.
510 https://doi.org/10.3390/atmos7100129

511 Coogan, S.C.P., Robinne, F.N., Jain, P., Flannigan, M.D., 2019. Scientists' warning on wildfire
512 — a canadian perspective. Can. J. For. Res. 49, 1015–1023. https://doi.org/10.1139/cjfr-
513 2019-0094

514 Donkelaar, A. Van, Martin, R. V., Li, C., Burnett, R.T., 2019. Regional Estimates of Chemical
515 Composition of Fine Particulate Matter Using a Combined Geoscience-Statistical Method
516 with Information from Satellites, Models, and Monitors. Environ. Sci. Technol. 53, 2595–
517 2611. https://doi.org/10.1021/acs.est.8b06392

518 Donkelaar, A. Van, Martin, R. V, Park, R.J., 2006. Estimating ground-level PM 2 . 5 using

519 aerosol optical depth determined from satellite remote sensing. J. Geophys. Res. Atmos.
520 111. https://doi.org/10.1029/2005JD006996

521 Donkelaar, A. Van, Martin, R. V, Spurr, R.J.D., Burnett, R.T., 2015. High-Resolution Satellite-
522 Derived PM2.5 from Optimal Estimation and Geographically Weighted Regression over
523 North America. Environ. Sci. Technol. 49, 10482–10491.
524 https://doi.org/10.1021/acs.est.5b02076

525 Dreessen, J., Sullivan, J., Delgado, R., 2016. Observations and impacts of transported Canadian
526 wildfire smoke on ozone and aerosol air quality in the Maryland region on June 9–12, 2015.
527 J. Air Waste Manag. Assoc. 66, 842–862. https://doi.org/10.1080/10962247.2016.1161674

528 EPA, 2018. Code of Federal Regulations Title 40: Protection of Environment 694.

529 EPA, 2011. Code of Federal Regulations Title 40: Protection of Environment 694.

530 Fotheringham, A.S., Charlton, M.E., Brunsdon, C., 1998. Geographically weighted regression: a
531 natural evolution of the expansion method for spatial data analysis. Environ. Plan. A 30,
532 1905–1927.

533 Fotheringham, S.A.., Brunsdon, C., Charlton, M., 2003. Geographically Weighted Regression :
534 The Analysis of Spatially Varying Relationships, John Wiley and Sons.

535 Freeborn, P.H., Wooster, M.J., Roy, D.P., Cochrane, M.A., 2014. Quantification of MODIS fire
536 radiative power (FRP) measurement uncertainty for use in satellite-based active fire
537 characterization and biomass burning estimation. Geophys. Res. Lett. 41, 1988–1994.
538 https://doi.org/10.1002/2013GL059086.

539 Geng, G., Meng, X., He, K., Liu, Y., 2020. Random forest models for PM 2 . 5 speciation

concentrations using MISR fractional AODs Random forest models for PM 2 . 5 speciation concentrations using MISR fractional AODs.

Geng, G., Murray, N.L., Tong, D., Meng, X., Chang, H.H., Liu, Y., Hu, X., Lee, P., 2018. Satellite-Based Daily PM 2 . 5 Estimates During Fire Seasons in Colorado 5. https://doi.org/10.1029/2018JD028573

Goldberg, D.L., Gupta, P., Wang, K., Jena, C., Zhang, Y., Lu, Z., Streets, D.G., 2019. Using gap-filled MAIAC AOD and WRF-Chem to estimate daily PM2.5 concentrations at 1 km resolution in the Eastern United States. Atmos. Environ. 199, 443–452. https://doi.org/10.1016/j.atmosenv.2018.11.049

Gu, Y., 2019. Estimating PM2 . 5 Concentrations Using 3 km MODIS AOD Products : A Case Study in British Columbia , Canada. University of Waterloo.

Guo, B., Wang, X., Pei, L., Su, Y., Zhang, D., Wang, Y., 2021. Identifying the spatiotemporal dynamic of PM2.5 concentrations at multiple scales using geographically and temporally weighted regression model across China during 2015–2018. Sci. Total Environ. 751. https://doi.org/10.1016/j.scitotenv.2020.141765

Gupta, P., Christopher, S.A., 2009a. Particulate matter air quality assessment using integrated surface, satellite, and meteorological products: 2. A neural network approach. J. Geophys. Res. Atmos. 114, 1–14. https://doi.org/10.1029/2008JD011497

Gupta, P., Christopher, S.A., 2009b. Particulate matter air quality assessment using integrated surface , satellite , and meteorological products : Multiple regression approach. J. Geophys. Res. Atmos. 114, 1–13. https://doi.org/10.1029/2008JD011496

561 Haarig, M., Ansmann, A., Baars, H., Jimenez, C., Veselovskii, I., Engelmann, R., Althausen, D.,
562 2018. Extreme levels of Canadian wildfire smoke in the stratosphere over central Europe –
563 Part 2: Lidar study of depolarization and lidar ratios at 355, 532, and 1064 nm and of
564 microphysical properties. Atmos. Chem. Phys. Discuss. 1–22. https://doi.org/10.5194/acp-
565 2018-358

566 Hessburg, P.F., Churchill, D.J., Larson, A.J., Haugo, R.D., Miller, C., Spies, T.A., North, M.P.,
567 Povak, N.A., Belote, R.T., Singleton, P.H., Gaines, W.L., Keane, R.E., Aplet, G.H.,
568 Stephens, S.L., Morgan, P., Bisson, P.A., Rieman, B.E., Salter, R.B., Reeves, G.H., 2015.
569 Restoring fire-prone Inland Pacific landscapes: seven core principles. Landsc. Ecol. 30,
570 1805–1835. https://doi.org/10.1007/s10980-015-0218-0

571 Hoff, R.M., Christopher, S.A., 2009. Remote Sensing of Particulate Pollution from Space : Have
572 We Reached the Promised Land ? J. Air Waste Manage. Assoc. 59, 645–675.
573 https://doi.org/10.3155/1047-3289.59.6.645

574 Hu, X., Belle, J.H., Meng, X., Wildani, A., Waller, L.A., Strickland, M.J., Liu, Y., 2017.
575 Estimating PM2.5 Concentrations in the Conterminous United States Using the Random
576 Forest Approach. Environ. Sci. Technol. 51, 6936–6944.
577 https://doi.org/10.1021/acs.est.7b01210

578 Hu, X., Waller, L.A., Al-Hamdan, M.Z., Crosson, W.L., Estes, M.G., Estes, S.M., Quattrochi,
579 D.A., Sarnat, J.A., Liu, Y., 2013. Estimating ground-level PM2.5 concentrations in the
580 southeastern U.S. using geographically weighted regression. Environ. Res. 121, 1–10.
581 https://doi.org/10.1016/j.envres.2012.11.003

582 Hu, Z., 2009. Spatial analysis of MODIS aerosol optical depth, PM2.5, and chronic coronary

583 heart disease. Int. J. Health Geogr. 8, 1–10. https://doi.org/10.1186/1476-072X-8-27

584 Hubbell, B.J., Crume, R. V., Evarts, D.M., Cohen, J.M., 2010. Policy Monitor: Regulation and
585 progress under the 1990 Clean Air Act Amendments. Rev. Environ. Econ. Policy 4, 122–
586 138. https://doi.org/10.1093/reep/rep019

587 Hystad, P., Demers, P.A., Johnson, K.C., Brook, J., Van Donkelaar, A., Lamsal, L., Martin, R.,
588 Brauer, M., 2012. Spatiotemporal air pollution exposure assessment for a Canadian
589 population-based lung cancer case-control study. Environ. Heal. A Glob. Access Sci.
590 Source 11, 1–22. https://doi.org/10.1186/1476-069X-11-22

591 J.A.Gillies, W.G.Nickling, G.H.Mctainsh, 1996. Dust concentration s and particle-size
592 characteristics of an intense dust haze event: inland delta region. Atmos. Environ. 30, 1081–
593 1090.

594 Jiang, M., Sun, W., Yang, G., Zhang, D., 2017. Modelling seasonal GWR of daily PM2.5 with
595 proper auxiliary variables for the Yangtze River Delta. Remote Sens. 9, 1–20.
596 https://doi.org/10.3390/rs9040346

597 Kearns, M., Ron, D., 1999. Algorithmic stability and sanity-check bounds for leave-one-out
598 cross-validation. Neural Comput. 11, 1427–1453.
599 https://doi.org/10.1162/089976699300016304

600 Koelemeijer, R.B.A., Homan, C.D., Matthijsen, J., 2006. Comparison of spatial and temporal
601 variations of aerosol optical thickness and particulate matter over Europe. Atmos. Environ.
602 40, 5304–5315. https://doi.org/10.1016/j.atmosenv.2006.04.044

603 Kollanus, V., Tiittanen, P., Niemi, J. V., Lanki, T., 2016. Effects of long-range transported air

pollution from vegetation fires on daily mortality and hospital admissions in the Helsinki metropolitan area, Finland. Environ. Res. 151, 351–358. https://doi.org/10.1016/j.envres.2016.08.003

Li, T., Shen, H., Yuan, Q., Zhang, X., Zhang, L., 2017. Estimating Ground-Level PM2.5 by Fusing Satellite and Station Observations: A Geo-Intelligent Deep Learning Approach. Geophys. Res. Lett. 44, 11,985-11,993. https://doi.org/10.1002/2017GL075710

Liang, F., Xiao, Q., Huang, K., Yang, X., Liu, F., Li, J., Lu, X., 2020. The 17-y spatiotemporal trend of PM2.5 and its mortality burden in China 117. https://doi.org/10.1073/pnas.1919641117

Liu, Y., Sarnat, J.A., Kilaru, V., Jacob, D.J., Koutrakis, P., 2005. Estimating ground-level PM2.5 in the eastern United States using satellite remote sensing. Environ. Sci. Technol. 39, 3269–3278. https://doi.org/10.1021/es049352m

Loader, C.R., 1999. BANDWIDTH SELECTION: CLASSICAL OR PLUG-IN? Ann. Stat. 27, 415–438.

Lyapustin, A., Korkin, S., Wang, Y., Quayle, B., Laszlo, I., 2012. Discrimination of biomass burning smoke and clouds in MAIAC algorithm. Atmos. Chem. Phys. 12, 9679–9686. https://doi.org/10.5194/acp-12-9679-2012

Lyapustin, A., Wang, Y., Korkin, S., Huang, D., 2018. MODIS Collection 6 MAIAC Algorithm. Atmos. Meas. Tech. 11, 5741–5765. https://doi.org/10.5194/amt-2018-141

Ma, Z., Hu, X., Huang, L., Bi, J., Liu, Y., 2014. Estimating ground-level PM2.5 in china using satellite remote sensing. Environ. Sci. Technol. 48, 7436–7444.

https://doi.org/10.1021/es5009399

Meixner, T., Wohlgemuth, P., 2004. Wildfire Impacts on Water Quality. J. Wildl. Fire 13, 27–35.

Melillo, J.M., Richmond, T., Yohe, G.W., 2014. Climate Change Impacts in the United States. Third Natl. Clim. Assess. 52. https://doi.org/10.7930/J0Z31WJ2.

Miao, Y., Liu, S., Guo, J., Huang, S., Yan, Y., Lou, M., 2018. Unraveling the relationships between boundary layer height and PM2.5 pollution in China based on four-year radiosonde measurements. Environ. Pollut. 243, 1186–1195. https://doi.org/10.1016/j.envpol.2018.09.070

Miller, D.J., Sun, K., Zondlo, M.A., Kanter, D., Dubovik, O., Welton, E.J., Winker, D.M., Ginoux, P., 2011. Assessing boreal forest fire smoke aerosol impacts on U.S. air quality: A case study using multiple data sets. J. Geophys. Res. Atmos. 116. https://doi.org/10.1029/2011JD016170

Mirzaei, M., Bertazzon, S., Couloigner, I., 2018. Modeling Wildfire Smoke Pollution by Integrating Land Use Regression and Remote Sensing Data : Regional Multi-Temporal Estimates for Public Health and Exposure Models. Atmosphere (Basel). 9, 335. https://doi.org/10.3390/atmos9090335

Munoz-alpizar, R., Pavlovic, R., Moran, M.D., Chen, J., Gravel, S., Henderson, S.B., Sylvain, M., Racine, J., Duhamel, A., Gilbert, S., Beaulieu, P., Landry, H., Davignon, D., Cousineau, S., Bouchet, V., 2017. Multi-Year (2013–2016) PM2.5 Wildfire Pollution Exposure over North America as Determined from Operational Air Quality Forecasts. Atmosphere (Basel). 8, 179. https://doi.org/10.3390/atmos8090179

647 Navarro, K.M., Schweizer, D., Balmes, J.R., Cisneros, R., 2018. A review of community smoke
648 exposure from wildfire compared to prescribed fire in the United States. Atmosphere
649 (Basel). 9, 1–11. https://doi.org/10.3390/atmos9050185

650 Samet, J.M., 2011. The clean air act and health - A clearer view from 2011. N. Engl. J. Med.
651 365, 198–201. https://doi.org/10.1056/NEJMp1103332

652 Sapkota, A., Symons, J.M., Kleissl, J., Wang, L., Parlange, M.B., Ondov, J., Breysse, P.N.,
653 Diette, G.B., Eggleston, P.A., Buckley, T.J., 2005. Impact of the 2002 Canadian forest fires
654 on particulate matter air quality in Baltimore City. Environ. Sci. Technol. 39, 24–32.
655 https://doi.org/10.1021/es035311z

656 Stephens, S.L., 2005. Forest fire causes and extent on United States Forest Service lands. Int. J.
657 Wildl. Fire 14, 213–222. https://doi.org/10.1071/WF04006

658 Trueblood, M.B., Lobo, P., Hagen, D.E., Achterberg, S.C., Liu, W., Whitefield, P.D., 2018.
659 Application of a hygroscopicity tandem differential mobility analyzer for characterizing PM
660 emissions in exhaust plumes from an aircraft engine burning conventional and alternative
661 fuels. Atmos. Chem. Phys. 18, 17029–17045. https://doi.org/10.5194/acp-18-17029-2018

662 U.S. Environmental Protection Agency, 2019. Particulate Matter (PM2.5) Trends.

663 Wang, H., Shi, G., Tian, M., Zhang, L., Chen, Y., Yang, F., Cao, X., 2017. Aerosol optical
664 properties and chemical composition apportionment in Sichuan Basin, China. Sci. Total
665 Environ. 577, 245–257. https://doi.org/10.1016/j.scitotenv.2016.10.173

666 Wei, J., Huang, W., Li, Z., Xue, W., Peng, Y., Sun, L., Cribb, M., 2019. Estimating 1-km-
667 resolution PM2.5 concentrations across China using the space-time random forest approach.

668 Remote Sens. Environ. 231, 111221. https://doi.org/10.1016/j.rse.2019.111221

669 Wei, J., Li, Z., Cribb, M., Huang, W., Xue, W., Sun, L., Guo, J., Peng, Y., Li, J., Lyapustin, A.,
670 Liu, L., Wu, H., Song, Y., 2020. Improved 1 km resolution PM2.5 estimates across China
671 using enhanced space–time extremely randomized trees. Atmos. Chem. Phys. 20, 3273–
672 3289.

673 Wei, J., Li, Z., Lyapustin, A., Sun, L., Peng, Y., Xue, W., Su, T., Cribb, M., 2021.
674 Reconstructing 1-km-resolution high-quality PM2.5 data records from 2000 to 2018 in
675 China: spatiotemporal variations and policy implications. Remote Sens. Environ. 252,
676 112136. https://doi.org/10.1016/j.rse.2020.112136

677 Xiao, Q., Chang, H.H., Geng, G., Liu, Y., 2018. An Ensemble Machine-Learning Model To
678 Predict Historical PM 2.5 Concentrations in China from Satellite Data.
679 https://doi.org/10.1021/acs.est.8b02917

680 Xu, T., Song, Y., Liu, M., Cai, X., Zhang, H., Guo, J., Zhu, T., 2019. Temperature inversions in
681 severe polluted days derived from radiosonde data in North China from 2011 to 2016. Sci.
682 Total Environ. 647, 1011–1020. https://doi.org/10.1016/j.scitotenv.2018.08.088

683 You, T., Wu, R., Huang, G., Fan, G., 2017. Regional meteorological patterns for heavy pollution
684 events in Beijing. J. Meteorol. Res. 31, 597–611. https://doi.org/10.1007/s13351-017-6143-
685 1

686 You, W., Zang, Z., Pan, X., Zhang, L., Chen, D., 2015. Estimating PM2.5 in Xi'an, China using
687 aerosol optical depth: A comparison between the MODIS and MISR retrieval models. Sci.
688 Total Environ. 505, 1156–1165. https://doi.org/10.1016/j.scitotenv.2014.11.024

689 You, W., Zang, Z., Zhang, L., Li, Y., Pan, X., Wang, W., 2016a. National-scale estimates of
690 ground-level PM2.5 concentration in China using geographically weighted regression based
691 on 3 km resolution MODIS AOD. Remote Sens. 8. https://doi.org/10.3390/rs8030184

692 You, W., Zang, Z., Zhang, L., Li, Y., Pan, X., Wang, W., 2016b. National-scale estimates of
693 ground-level PM2.5 concentration in China using geographically weighted regression based
694 on 3 km resolution MODIS AOD. Remote Sens. 8, 184. https://doi.org/10.3390/rs8030184

695 Zhang, H., Hoff, R.M., Engel-Cox, J.A., 2009. The relation between moderate resolution
696 imaging spectroradiometer (MODIS) aerosol optical depth and PM2.5 over the United
697 States: A geographical comparison by U.S. Environmental Protection Agency regions. J.
698 Air Waste Manag. Assoc. 59, 1358–1369. https://doi.org/10.3155/1047-3289.59.11.1358

699 Zhang, H., Wang, Y., Hu, J., Ying, Q., Hu, X.M., 2015. Relationships between meteorological
700 parameters and criteria air pollutants in three megacities in China. Environ. Res. 140, 242–
701 254. https://doi.org/10.1016/j.envres.2015.04.004

702 Zheng, C., Zhao, C., Zhu, Y., Wang, Y., Shi, X., Wu, X., Chen, T., Wu, F., Qiu, Y., 2017.
703 Analysis of influential factors for the relationship between PM2.5 and AOD in Beijing.
704 Atmos. Chem. Phys. 17, 13473–13489. https://doi.org/10.5194/acp-17-13473-2017

705 Zhu, Y., Hinds, W.C., Kim, S., Sioutas, C., 2002. Concentration and size distribution of ultrafine
706 particles near a major highway. J. Air Waste Manag. Assoc. 52, 1032–1042.
707 https://doi.org/10.1080/10473289.2002.10470842

708 Zou, B., Pu, Q., Bilal, M., Weng, Q., Zhai, L., Nichol, J.E., 2016. High–resolution Satellite
709 Mapping of Fine Particulates Based on Geographically Weighted Regression. Ieee Geosci.
710 Remote Sens. Lett. 13, 495–499.

711
712
713
714
715
716
717
718
719
720
721
722
723
724
725
726

727 Table 1. Datasets used in the study with sources.

728

	Data /Model	Sensor	Spatial Resolution	Temporal Resolution	Accuracy
1	Surface $PM_{2.5}$	TEOM	Point data	daily	±5~10%
2	Mid visible aerosol optical depth (AOD)	MAIAC_ MODIS	1km	daily	66% compared to AERONET
3	Fire Radiative Power (FRP)	Terra/Aqua-MODIS	1km	daily	± 7%
4	ECMWF (Meteorological variables)		0.25 degree	hourly	

729 1) https://www.epa.gov/outdoor-air-quality-data

730 2) https://earthdata.nasa.gov/

731 3) https://earthdata.nasa.gov/

732 4) https://www.ecmwf.int/en/forecasts

733

734

735

736 Table 2. Total FRP in Canada and Northwestern US in August of Different Years (unit: 10^4

737 MW)

Year	2010	2011	2012	2013	2014	2015	2016	2017	2018
CA	148.24	4.84	19.93	70.54	107.78	10.39	4.6	307.3	542.99
NW US	16.41	42.84	320.39	192.06	67.01	339.58	112.9	195.64	296.91

738

739 Table 3. statistics of 15 states that violate EPA standards (35 $\mu g\ m^{-3}$) during the 17-day wildfire
740 period

State	number of site violate standard	number of site in the state	Percentage of site violate standard (%)	number of days violate standard
Montana	14	15	93.34	16
Washington	18	20	90	16
Oregon	12	14	85.71	5
North Dakota	7	11	63.63	4
Idaho	5	8	62.5	8
Colorado	11	21	52.38	2
South Dakota	5	10	50	1
California	57	119	47.9	14
Utah	7	15	46.67	4
Nevada	4	13	30.77	1
Wyoming	7	24	29.2	2
Minnesota	4	26	15.4	2
Texas	3	37	8.1	1
Louisiana	1	14	7.1	1
Arizona	1	20	5	1

741

742 Table 4. Coefficients of different predictors

Mean coefficients	sample selection	N	AOD	smoke flag	PBL	T2M	RH	U	SP
box1(red)	FRP>1000	213	91.94	-0.14	-2.25	0.33	0.08	-2	-0.06
box2(gold)	PM2.5>30	362	60.1	0.013	-2.9	0.23	-0.08	-1.6	-0.03
box3(green)	PM2.5>17	278	6.2	0.05	0.2	0.2	0.014	-0.3	-0.02
box4(black)	17>PM2.5>10	938	7.1	-0.02	-1.2	0.22	-0.035	0.06	-0.005
whole US region	~	106352	28.1	0.024	-0.9	0.06	-0.04	-0.7	-0.002

743

744

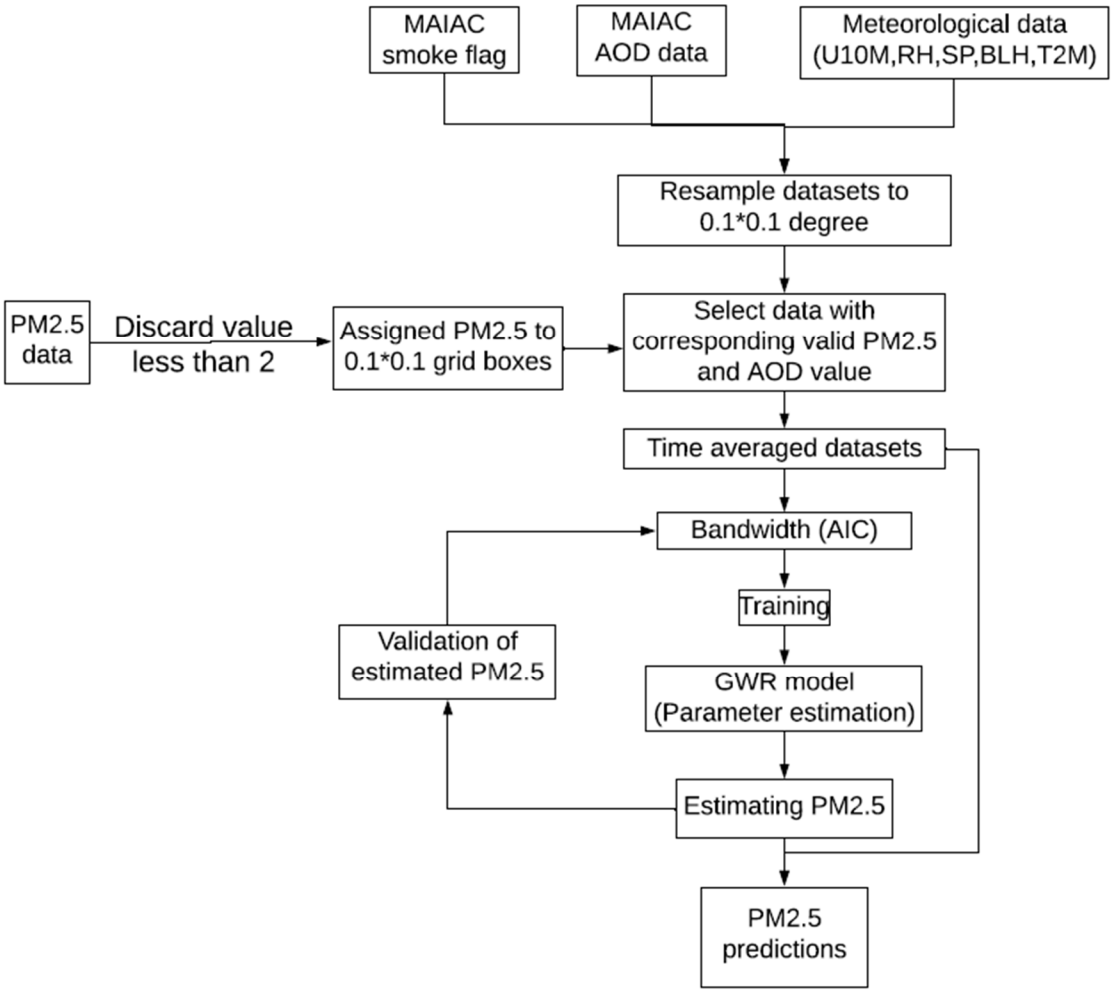

745

746 Figure 1. Flow chart for the Geographically Weighted Regression model used. All satellite,

747 ground, meteorological data are gridded to 0.1 by 0.1 degrees.

748

749

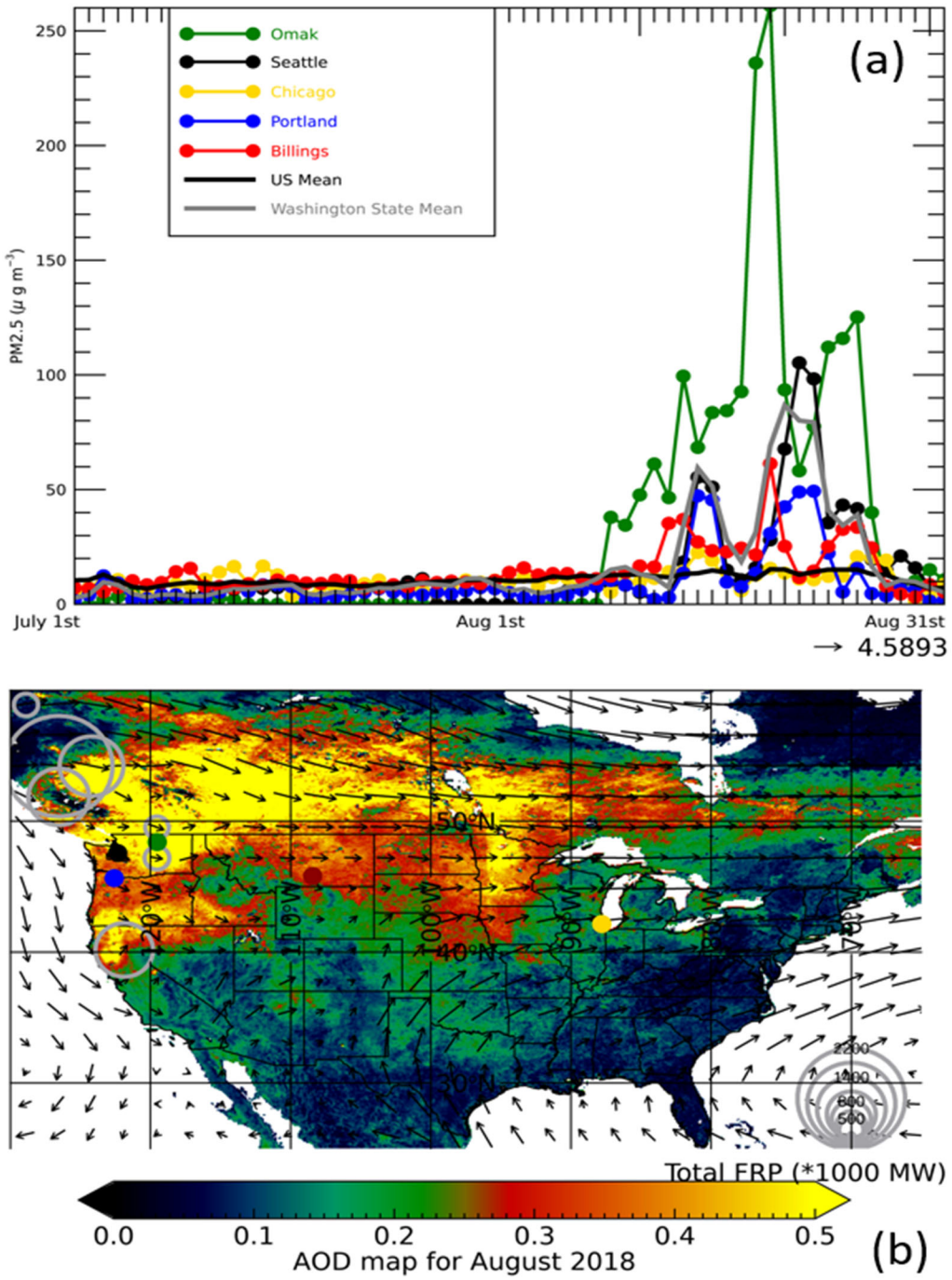

Figure 2. (a) Variations of EPA ground observed $PM_{2.5}$ in different cities from July to August 2018 (Omak-Washington, Seattle-Washington, Chicago-Illinois, Portland-Oregon, Billings-Montana). Black line without markers shows the mean variation of the whole US stations and the grey line without markers shows the mean variation of stations in Washington state. (b) Mean MAIAC satellite AOD distribution from August 9th to August 25th, 2018. AOD values equal or larger than 0.5 are shown as the same color (yellow). Also shown are circles with Fire Radiative Power (FRP). Black arrow shows the wind direction and the length of it represents the wind speed. The round spots of different colors on the map show the locations of the five selected cities (green-Omak, black-Seattle, yellow-Chicago, blue-Portland, red-Billings).

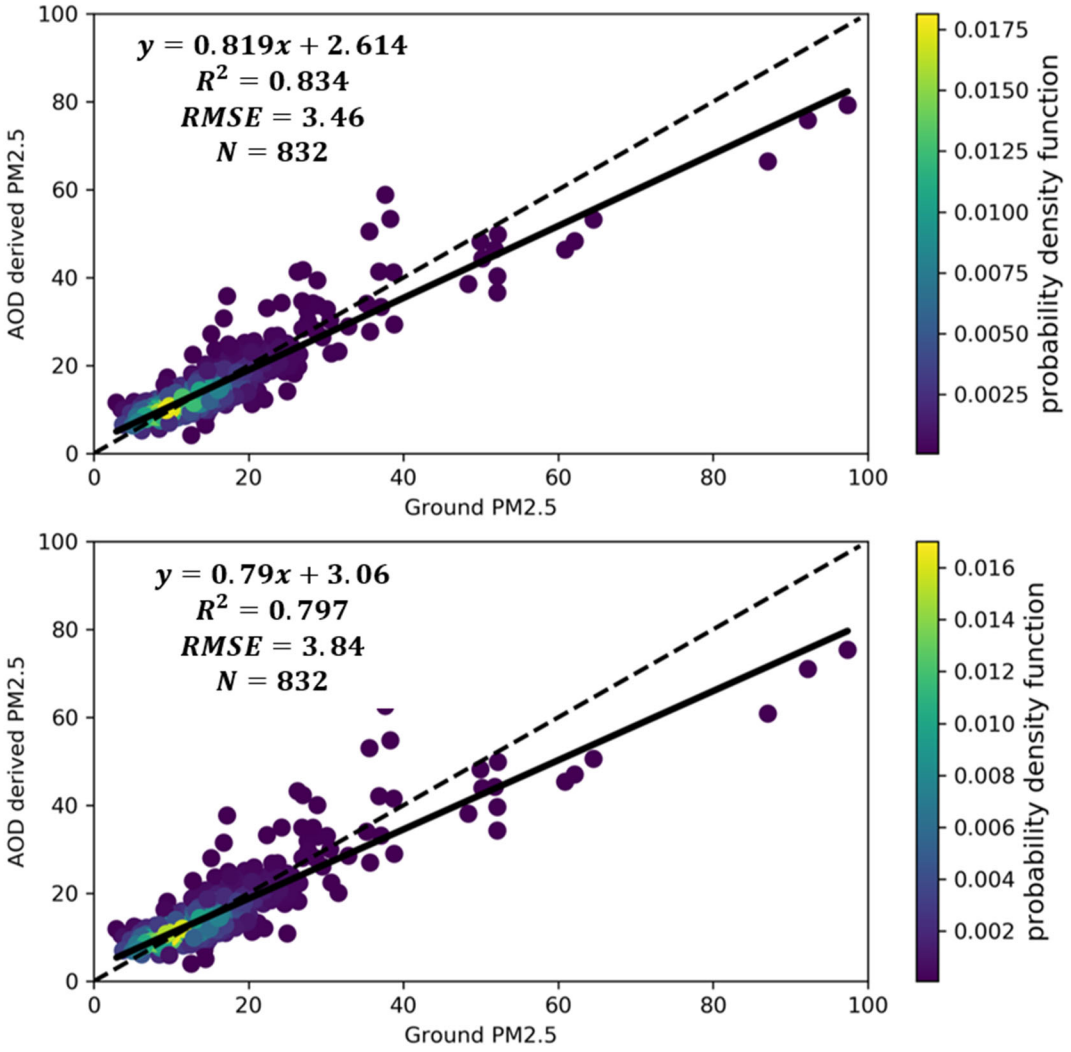

Figure 3. Results of model fitting and cross validation for GWR model for the entire US region averaged from August 9th to August 25th, 2018. (a) GWR model fitting results (b) GWR model LOOCV results. The dash line is the 1:1 line as reference and the black line shows the regression line. The color of the scatter plots represents the probability density function which provides a relative likelihood that the value of the random variable would equal a certain sample.

774

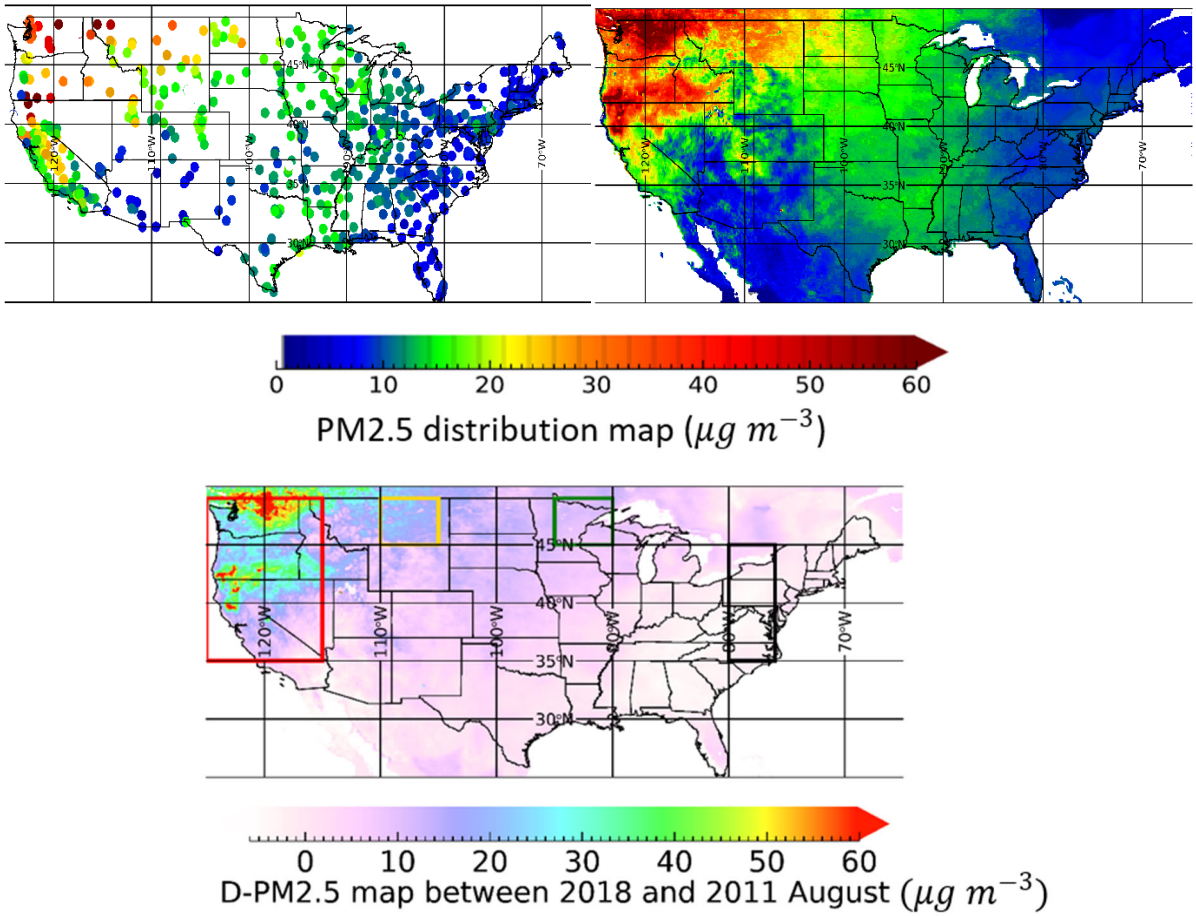

775

776

777

778 Figure 4. (a) EPA ground observed $PM_{2.5}$ distribution over the US averaged from August 9th to
779 August 25th, 2018. (b) GWR predicted 17-day mean $PM_{2.5}$ distribution. (c) Difference map of
780 predicted ground $PM_{2.5}$ of the 17-day mean values between 2018 and 2011. $PM_{2.5}$ values equal or
781 larger than 60 $\mu g\ m^{-3}$ are shown as the same color (red). Note that the D-$PM_{2.5}$ has a different
782 color scale to make the negative values more apparent (blue).
783

784

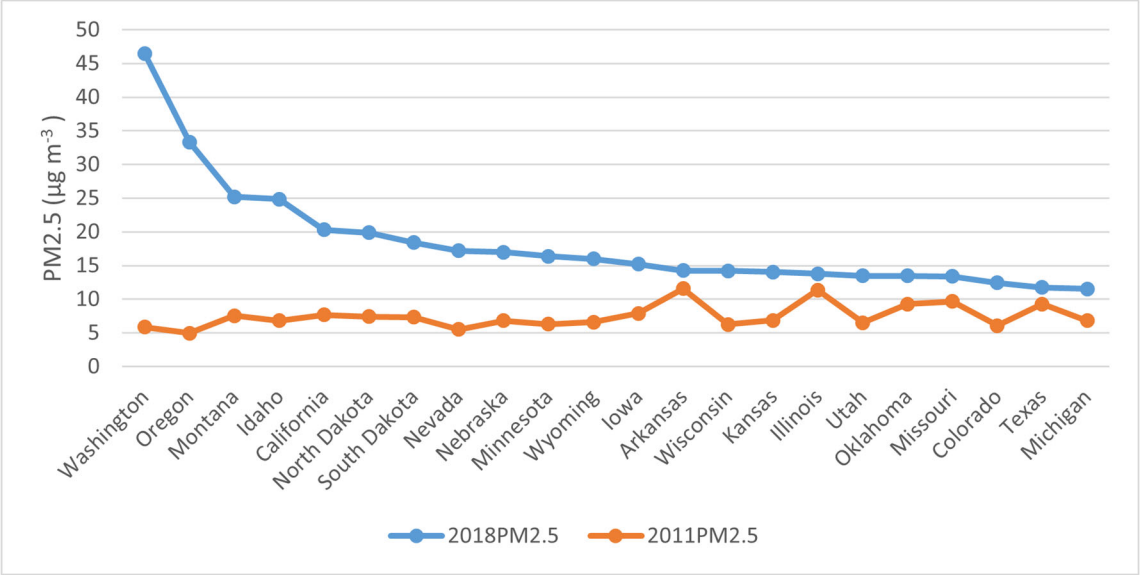

Figure 5. Mean $PM_{2.5}$ from August 9th to August 25th in 2018 and 2011 of most affected states

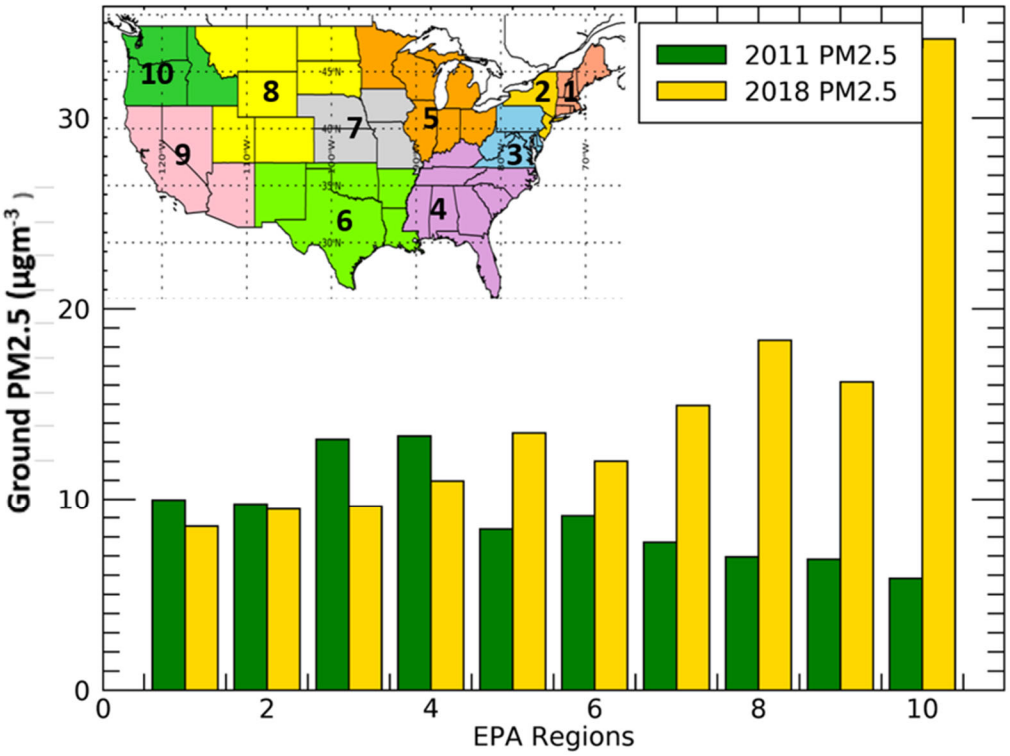

790 Figure 6. Mean $PM_{2.5}$ of EPA regions from August 9th to August 25th in 2011 and 2018. Inset
791 shows the map of 10 EPA regions in different colors. Yellow column represents the 2018 mean
792 $PM_{2.5}$ and green column represents for 2011 mean $PM_{2.5}$.

793

794